SF2A 2019
P. Di Matteo, O. Creevey, A. Crida, G. Kordopatis, J. Malzac, J.-B. Marquette, M. N'Diaye, O. Venot (eds)

MAGNETIC HIDE & SEEK IN THE KEPLER-78 SYSTEM: WIND MODELLING AND STAR-PLANET MAGNETIC INTERACTIONS

A. Strugarek[1], J. Ahuir[1], A. S. Brun[1], J.F. Donati[2], C. Moutou[2] and V. Réville[2]

Abstract. Observational evidences for star-planet magnetic interactions (SPMIs) in compact exosystems have been looked for in the past decades. Their theoretical description has significantly progressed in the past years. Nevertheless, their complete description requires a detailed knowledge of the host star, and in particular its coronal magnetic and plasma characteristics. We explore here the robustness of SPMIs models with respect to the basic coronal properties commonly assumed for cool stars, in the particular context of the Kepler-78 system. We show that the amplitude of SPMIs is constrained only within one to two orders of magnitude as of today. However, the temporal signature of SPMIs can be robustly predicted from models, paving the road toward their future detection in compact exosystems through dedicated observational strategies.

Keywords: planet-star interactions – stars: wind, outflows – magnetohydrodynamics (MHD)

1 Introduction

Planets on short-period orbit around cool stars interact strongly with their host in a variety of physical processes: gravitational (tidal) interaction (Mathis 2017), stellar irradiation (e.g. Daley-Yates & Stevens 2019), and star-planet magnetic interaction (SPMI, Strugarek 2018). The latter occurs when the planet orbital path is within the Alfvén surface of the star, which is the characteristic surface at which the accelerating wind of the star reaches the local Alfvén speed and becomes super-Alfvénic.

Recently, Cauley et al. (2019) showed evidences of tracers of SPMIs in the CaII K line for four observed compact exosystems. Among the compact exosystems, ultra-short period planets (Winn et al. 2018) such as Kepler-78b are particularly favorable candidates to exhibit traces of SPMIs. Nevertheless, the unambiguous detection of SPMIs requires *a priori* a detailed knowledge of the star and the planet. Indeed, the temporal traces of SPMIs are primarily controlled by the magnetic field amplitude and topology of the hosting star (Strugarek et al. 2015). Their amplitude is in turn controlled by both the magnetic properties of the star and the magnetic (or lack of thereof) properties of the orbiting planet (Saur et al. 2013; Strugarek 2016).

The ultra-short period system Kepler-78 was recently modelled in 3D by Strugarek et al. (2019). The corona and wind of Kepler-78 was modelled under the magnetohydrodynamic (MHD) framework to assess the properties of SPMIs in this system. Their modelling made use of an observed magnetic map of Kepler-78 for this period (Moutou et al. 2016). It allows detailed estimates of the SPMI properties along the planetary orbit. They found that SPMIs could carry a sufficient amount of energy to be detectable with present telescope capabilities. This study shed the light on the importance of considering the 3D magnetic topology of the star to accurately predict and identify the complex temporal signture of SPMIs in compact exosystems.

In this proceeding we explore the robustness of the results of Strugarek et al. (2019) with respect to their wind modelling assumptions. In particular, the detection of stellar wind and the associated mass loss rate is extremely challenging (e.g. Wood et al. 2005). As a result, modelling the wind of a given star requires today some assumption on, *e.g.* the density and temperature at the base of their corona. Even though some aspects of these plasma characteristics can be constrained through observations (for in-depth discussions, see Ahuir et al. 2019), we still have today quite some liberty in setting these parameters. We henceforth discuss these modelling choices for Kepler-78 in Section 2, and their implication for our estimates of SPMIs in Section 3. We finally conclude our study in Section 4.

[1] AIM, CEA, CNRS, Université Paris-Saclay, Université Paris Diderot, Sorbonne Paris Cité, F-91191 Gif-sur-Yvette, France
[2] Université de Toulouse / CNRS-INSU, IRAP / UMR 5277, F-31400 Toulouse, France

2 Modelling the environment of Kepler-78

2.1 A 1D+3D stellar wind model

We model the corona and wind of Kepler-78 following a 1D+3D approach developed in Strugarek et al. (2019). The model is based on a 1D polytropic Parker-like solution stellar wind. It assumes a given density and temperature at the base of the corona (the chosen values are discussed in Section 2.2) to compute a spherically-symmetric wind solution for Kepler-78.

A purely spherically-symmetric solution is nevertheless not precise enough to properly model SPMIs (Strugarek et al. 2015). We consequently leverage our knowledge of the global magnetic topology of Kepler-78 deduced from Zeeman-Doppler Imaging by Moutou et al. (2016). We then extrapolate the coronal magnetic field with a potential field source-surface technique (e.g. see Schrijver & DeRosa 2003). Réville et al. (2015) developed an estimate of the optimal source-surface radius $R_{\rm ss}^{\rm opt}$ that allows to reproduce as close a possible the coronal topology obtained from a fully 3D MHD modelling. In the case of Kepler-78 we find $R_{\rm ss}^{\rm opt} \in [4.8R_\star, 7.R\star]$ in the parameter space we explored (see Section 2.2).

Combined with the spherically-symmetric wind solution, this coupled 1D-3D approach was shown to reproduce satisfyingly the low corona of fully 3D MHD models for Kepler-78 (Strugarek et al. 2019). We note here that this technique breaks close to the source-surface and beyond. Henceforth, we use it here to model Kepler-78 low corona at the planetary orbit ($R_{\rm orb} < R_{\rm ss}$), but it cannot *a priori* be generically used for any close-in planet.

2.2 Coronal parameters for Kepler-78

Star Kepler-78	
$T_{\rm eff}$ $[K]$	5089 ± 50
$M_\star$ $[M_\odot]$	0.81 ± 0.08
$R_\star$ $[R_\odot]$	0.74 +0.1,-0.08
$P_{\rm rot}$ [days]	12.5
Planet Kepler-78b	
R_p $[R_\oplus]$	1.16 +0.19,-0.14
M_p $[M_\oplus]$	1.86 ± 0.25
$P_{\rm orb}$ [days]	0.36
Semi-major axis $[R_\star]$	2.66

Table 1. Global properties of the Kepler-78 system. Values were taken from Sanchis-Ojeda et al. (2013); Pepe et al. (2013); Howard et al. (2013).

The basic stellar and planetary parameters of the Kepler-78 system are given in Table 1. Modelling the wind and corona of a distant star generally further requires to estimate the density and temperature at the base of the corona. These two quantities are not easily constrained through observations (*e.g.* Johnstone & Güdel 2015), and a choice has generally to be made. Holzwarth & Jardine (2007) proposed that the coronal proton density and temperature should scale with the stellar rotation rate $\Omega_\star$ of the star such that

$$n_c \simeq n_\odot \left(\frac{\Omega_\star}{\Omega_\odot}\right)^{0.6} \quad \text{and} \quad T_c \simeq T_\odot \left(\frac{\Omega_\star}{\Omega_\odot}\right)^{0.1}, \tag{2.1}$$

which leads to $n_c = 1.6 \times 10^8$ cm^{-3} and $T_c = 1.63$ MK for Kepler-78.

This approach was followed in Strugarek et al. (2019) to model the corona of Kepler-78. Nevertheless, assuming a given mass-loss rate for Kepler-78, this choice of coronal density is not unique. For instance, Johnstone & Güdel (2015) derived a scaling law for the closed loop coronal temperature based on the X-ray luminosity of the star that can be written as

$$T_{\rm cor} = T_{\rm cor}^\odot \left(\frac{M_\star}{M_\odot}\right)^{-0.42} \left(\frac{\Omega_\star}{\Omega_\odot}\right)^{0.52}, \tag{2.2}$$

where in their notation $T_{\rm cor}^{\odot} = 0.94$ MK. This relationship gives $T_{\rm cor} = 1.56$ MK for Kepler-78. If one assumes that the closed coronal loop temperature gives a satisfying proxy for the open field lines regions, this estimate gives a slightly cooler corona than the Holzwarth & Jardine (2007) prescription 2.1. Nevertheless, with this approach the coronal density still needs to be prescribed.

In this proceeding we aim to assess the impact of our wind modelling on our ability to estimate and predict the characteristics of star-planet magnetic interactions. As a result, we explore a somewhat broad range of coronal temperatures $T_c \in [1.15, 5]$ MK for Kepler-78. We then follow two strategies:

- We maintain the density constant to the canonical value $n_c = 1.6 \times 10^8$ cm^{-3} chosen in Strugarek et al. (2019).
- We maintain the mass loss rate to the canonical value of 2.88×10^{-14} $M_\odot$/yr chosen in Strugarek et al. (2019). The coronal density n_c is chosen to maintain a constant mass loss rate with the approximate mass-loss equation (Lamers & Cassinelli 1999)

$$\dot{M} \propto M_\star^2 n_c T_c^{-3/2} \left[1 - \frac{T_{\rm min,\odot}}{T_c}\frac{M_\star}{M_\odot}\frac{R_\odot}{R_\star}\right]^{\frac{5-3\gamma}{2(\gamma-1)}} , \tag{2.3}$$

  where γ the polytropic index of the modelled wind, and $T_{\rm min,\odot} \simeq 11(1-1/\gamma)$ (for more details, see Ahuir et al. 2019).

We illustrate the resulting wind speed profiles in Fig. 1 for three representative cases in each approach. On the left panel we show the profiles for a constant mass-loss rate. As the coronal density varies by 2 orders of magnitude, the wind speed at the average Alfvén radius r_A (dots in Fig. 1) varies by about a factor of 3. The average Alfvén radius itself does not change significantly because we fixed the mass loss rate to a constant value here.

In the right panel of Fig. 1, the base coronal density n_c is held constant. Similarly, the wind speed at the average Alfvén radius varies by factor 2 to 3 while the mass-loss rate varies by 2 orders of magnitude. In this case the average Alfvén radius changes significantly from $6R_\star$ to $11.6R_\star$ when the mass loss is multiplied by 100.

It is worth to note that the planet is found to orbit within the sub-Alfvénic region of the wind (*i.e.* below r_A) in all cases. This does not necessarily imply that the interaction between the planet and the stellar wind is sub-Alfvénic, because the orbital motion of the planet can be super-Alfvénic itself (this will be made clear in Section 3, the interested reader will find more in depth-discussion on this aspect in Vidotto et al. 2010; Strugarek 2018).

For all the scenarii, the plasma characteristics change in the corona and hence change as well at the planetary orbit. We can thus expect that these different choices of modelling will have an impact on our estimates of star-planet magnetic interactions. We now quantify this impact in Section 3.

3 Impact of the stellar wind modelling on star-planet magnetic interaction properties

SPMIs are first determined by the *relative* Alfvénic Mach number which is defined as

$$M_a = \frac{|\mathbf{v}_w - \mathbf{v}_{\rm kep}|}{v_a} , \tag{3.1}$$

where $\mathbf{v}_w$ is the stellar wind speed, $\mathbf{v}_{\rm kep}$ is the keplerian speed of the orbiting planet, and v_a is the Alfvén speed in the stellar wind. M_a is shown as a function of the orbital phase $\phi_{\rm orb}$ and the coronal parameters in the top left panel of Fig. 2. The left axis labels the coronal density n_c, and the right axis the coronal temperature T_c. We show here the results for the constant-$\dot{M}_\star$ parameter-space exploration. We see that M_a varies by a factor 5 as the coronal density is increased by an order of magnitude. Interestingly, for high densities M_a becomes larger than 1 around $\phi_{\rm orb} \simeq 0.25$ while the average Alfvén radius remains around 8 $R_\star$ (see left panel in Fig. 1). This means that the relative keplerian motion becomes super-Alfvénic, because the local alfvén speed of the wind decreases significantly as the coronal density increases.

The energy available for SPMIs then depends on the stellar wind Poynting flux density

$$S_w = |\mathbf{v}_w - \mathbf{v}_{\rm kep}| \frac{B_w^2}{\mu_0} \sin(\Theta_0) \tag{3.2}$$

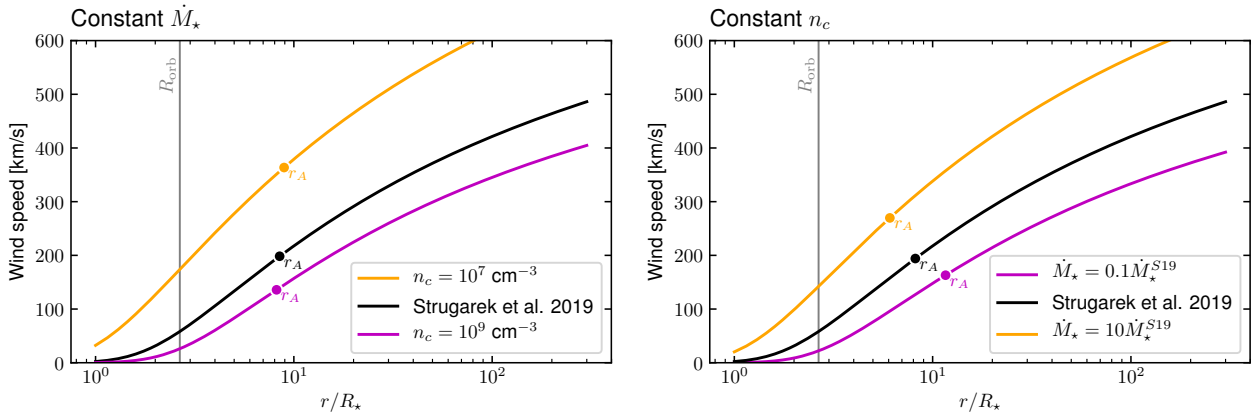

Fig. 1. Radial velocity profile of a polytropic Parker-like wind. On the left, the density and temperature at the base of the corona are changed while the mass loss-rate is held constant. On the right, the density at the base of the corona is held fixed, while the coronal temperature is altered (and thus the wind mass loss rate changes). The average Alfvén radius is labelled by the coloured dot on each curve. The black lines represent the modelling choices made in Strugarek et al. (2019). Two other modelling choices are illustrated in orange and magenta on each panel.

intercepted by the planet, where B_w is the local magnetic field amplitude and Θ_0 is the inclination of the wind magnetic field with respect to the orbital motion. The Poynting flux density is shown on the top right panel of Fig. 2. The available Poynting flux density shows no dependancy on the chosen coronal density. This is due to the fact that we chose to explore the parameter-space with a fixed mass-loss, which leads to a fixed open-flux and hence a fixed magnetic structure in the corona as the plasma parameters are varied (see Réville et al. 2015).

Thanks to our SPMI modelling we can estimate the minimal magnetic dipole $B_{\rm min}$ Kepler-78b needs to sustain a magnetosphere (bottom left panel in Fig. 2), as well as the Poynting flux $\mathcal{P}$ channeled by the interaction from the planetary orbit towards Kepler-78 (bottom right panel, for the full formulation of $\mathcal{P}$ see Strugarek 2017). We see that both quantities vary by one to two orders of magnitude as the coronal density increases by three orders of magnitude.

The wind modelling choices –namely the prescribed density and temperature at the base of the corona of Kepler-78– heavily influences the estimated *amplitude* of SPMI. Nonetheless, the relative variations of $B_{\rm min}$ and $\mathcal{P}$ along the planetary orbit remain remarkably similar as the parameter space is explored (albeit their absolute value differ). These two aspects were also found in the second parameter-space exploration (constant n_c), we did not illustrate them here for the sake of brevity.

4 Conclusions

In this proceeding we have studied the influence of wind-modelling parameters on estimates of star-planet magnetic interactions. In particular, we have focused our discussion on the choice of plasma density and temperature at the base of the corona. We have illustrated here this dependancy in the context of Kepler-78. This system has been modeled in details in Strugarek et al. (2019) with one possible choice of plasma parameters at the base of the stellar corona. We have explored a large parameter-space following two strategies: keeping a constant density at the base of the corona (and thus exploring five orders of magnitude in mass-loss rate), and keeping a constant wind mass-loss rate (and thus exploring four orders of magnitude in coronal density).

On one hand, we found that the important plasma parameters for SPMIs are very sensitive to the wind modelling choice. This leads to a typical uncertainty of one to two orders of magnitude in the power channeled by the SPMI in systems such as Kepler-78. On the other hand, the temporal variability of the signal is much less sensitive to the wind modelling choices as long as the overall coronal magnetic topology is known. This was already hinted in Strugarek et al. (2019) and opens up promising research avenues to properly characterize observable signatures of SPMIs in compact systems (see Cauley et al. 2019, for a recent attempt in this direction).

A.S. and A.S.B. acknowledge funding from CNES-PLATO and CNES-Space Weather grants. A.S. and A.S.B. acknowledge funding from the Programme National Soleil-Terre (PNST). A.S. acknowledges funding from the Programme National de Planétologie

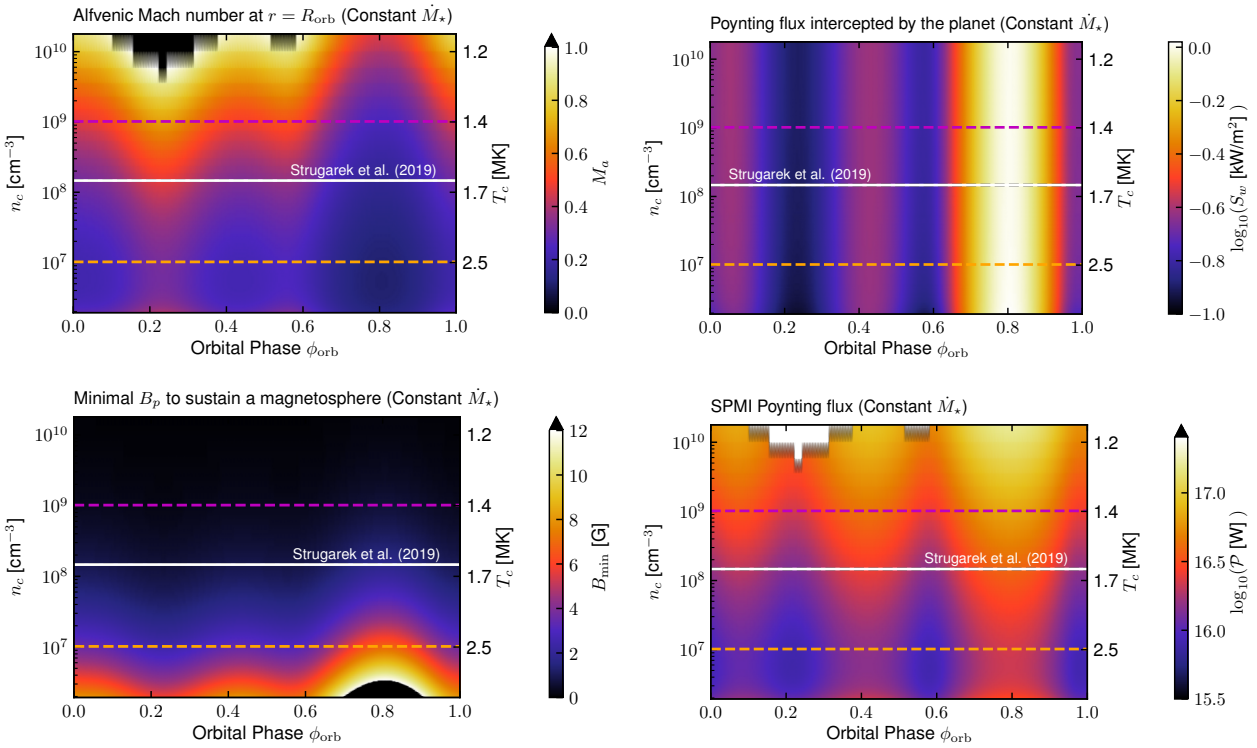

Fig. 2. SPMI characteristics for varying density and temperature at the base of the corona of Kepler-78, at constant $\dot{M}_\star$. From top left to bottom right, we show the relative Alfvénic Mach number M_a, the Poynting flux density intercepted by the Kepler-78b, the minimal dipolar field $B_{\rm min}$ of Kepler-78b required to sustain a magnetosphere, and the Poynting flux $\mathcal{P}$ channeled by the SPMI toward Kepler-78. Each panel follows the same layout: the x-axis represents the orbital phase $\phi_{\rm orb}$ of Kepler-78b, the left y-axis the assumed coronal density, and the right y-axis the assumed coronal temperature. The horizontal white line correspond to the wind model of Strugarek et al. (2019). The dashed orange and magneta lines correspond to the orange and magenta lines in Fig. 1 ($n_c = 10^7$ cm^{-3} and 10^9 cm^{-3}, respectively).

(PNP). J.F.D. acknowledges funding from the European Research Council (ERC) under the H2020 research & innovation program (grant agreement #740651 NewWorlds).

References

Ahuir, J., Brun, A. S., & Strugarek, A. 2019, Submitt. to A&A
Cauley, P. W., Shkolnik, E. L., Llama, J., & Lanza, A. F. 2019, Nat. Astron., 1
Daley-Yates, S. & Stevens, I. R. 2019, MNRAS, 483, 2600
Holzwarth, V. & Jardine, M. 2007, Astron. Astrophys., 463, 11
Howard, A. W., Sanchis-Ojeda, R., Marcy, G. W., et al. 2013, Nature, 503, 381
Johnstone, C. P. & Güdel, M. 2015, Astron. Astrophys., 578, A129
Lamers, H. J. G. L. M. & Cassinelli, J. P. 1999, Introduction to Stellar Winds
Mathis, S. 2017, in Handb. Exopl. (Springer International Publishing), 1–30
Moutou, C., Donati, J.-F., Lin, D., Laine, R. O., & Hatzes, A. 2016, Mon. Not. R. Astron. Soc., 459, 1993
Pepe, F., Cameron, A. C., Latham, D. W., et al. 2013, Nature, 503, 377
Réville, V., Brun, A. S., Strugarek, A., et al. 2015, Astrophys. J., 814, 99
Sanchis-Ojeda, R., Rappaport, S., Winn, J. N., et al. 2013, Astrophys. J., 774, 54
Saur, J., Grambusch, T., Duling, S., Neubauer, F. M., & Simon, S. 2013, Astron. Astrophys., 552, A119
Schrijver, C. J. & DeRosa, M. L. 2003, Sol. Phys., 212, 165
Strugarek, A. 2016, Astrophys. J., 833, 140
Strugarek, A. 2017, EWASS Spec. Sess. 4 Star-planet Interact.

Strugarek, A. 2018, in Handb. Exopl. (Cham: Springer International Publishing), 1833–1855
Strugarek, A., Brun, A. S., Donati, J.-F., Moutou, C., & Réville, V. 2019, Astrophys. J., 881, 136
Strugarek, A., Brun, A. S., Matt, S. P., & Réville, V. 2015, Astrophys. J., 815, 111
Vidotto, A. A., Jardine, M., & Helling, C. 2010, Astrophys. J. Lett., 722, L168
Winn, J. N., Sanchis-Ojeda, R., & Rappaport, S. 2018, New Astron. Rev., 83, 37
Wood, B. E., Müller, H.-R., Zank, G. P., Linsky, J. L., & Redfield, S. 2005, Astrophys. J., 628, L143